Int. J. Electrochem. Sci., 17 **(2022)** Article Number: 220647, doi: 10.20964/2022.06.52

International Journal of
ELECTROCHEMICAL
SCIENCE
www.electrochemsci.org

Short Communication

Hydrothermal Synthesis of GO/Pd/ZnO nanocomposite as Photocatalyst for Enhanced Photocatalytic Degradation of Azo Dye under Ultraviolet Light Irradiation

Lixiu Liu[*], *Aijiang He, Xia Yao*

School of New Materials and Chemical Energy, YiBin Vocational And Technical College, Yibin 644003, China
[*]E-mail: Liulixiu2020@163.com

Received: 15 February 2022 / *Accepted:* 16 April 2022 / *Published:* 7 May 2022

The current research focuses on the hydrothermal production of a nanocomposite based on graphene oxide and Pd/ZnO nanorodes (GO/Pd/ZnO) for the photocatalytic degradation of Direct Red 23 (DR23) from textile effluent under UV light irradiation. XRD and SEM analyses revealed that the Pd/ZnO nanorods were anchored onto the crumpled-like characteristics of GO nanosheets in the GO/Pd/ZnO nanocomposite. The optical band gap values for ZnO nanorods, Pd/ZnO nanorods, and GO/Pd/ZnO nanocomposite were found to be 3.10, 3.01, and 2.95 eV, respectively, showing that the GO/Pd/ZnO nanocomposite exhibits a lower band gap than pure ZnO and Pd/ZnO nanorods. EIS measurements revealed a reduction in charge transfer resistance with the addition of Pd and GO nanosheets to the ZnO structure. The photocatalytic performance of photocatalysts for the degradation of 100 ml of 80 mg/l DR23 solution under UV light irradiation revealed that after 60 minutes of UV light irradiation, ZnO nanorods, Pd/ZnO nanorods, and GO/Pd/ZnO nanocomposite achieved 63.0%, 75.9%, and 84.7% DR23 degradation efficiency, respectively. The complete treatment is achieved after 145, 125, and 120 minutes of UV light irradiation on ZnO nanorods, Pd/ZnO nanorods, and GO/Pd/ZnO nanocomposite, respectively, indicating the high photocatalytic efficiency of GO/Pd/ZnO nanocomposite compared to other photocatalysts reported in the literature due to synergetic action between GO, Pd, and ZnO The produced photocatalysts in this study were found to be effective in treating the DR23 pollutant in textile wastewater.

Keywords: GO/Pd/ZnO; Nanocomposite; Hydrothermal; Direct Red 23; Photocatalytic degradation; Electrochemical impedance spectroscopy

1. INTRODUCTION

The most common synthetic colorants are direct azo dyes, which are widely used in the textile, cotton, paper, leather, wool, silk, nylon, printing, and paper industries [1-3]. They're also employed as biological stains and pH indicators. Direct dyes are also utilized in low-cost viscose or mixed curtain

textiles, upholstery, and carpets [4, 5]. Because of their good substantial properties for cellulosic textile materials like cotton and viscose rayon, direct dyes are also known as substantive dyes [6, 7]. This group of dyes gets its name from the fact that they have a direct affinity for cellulose fibers when applied from an aqueous solution [8-10].

Direct dyes have high water solubility, making it difficult to remove them using traditional procedures [11-13]. Color pollution from industrial and textile dyes causes not only aesthetic damage to bodies of water, but also reduces light penetration into the water, preventing submerged plants and algae from capturing the necessary light for photosynthesis and lowering dissolved oxygen levels, which is a dangerous situation for aquatic ecosystems [14-16]. Furthermore, they have been proven to include carcinogens, function as toxic and mutagenic agents, and can induce allergies such as contact dermatitis and respiratory disorders, as well as allergic reactions in the eyes, skin irritation, and irritation of the mucous membrane and upper respiratory tract [17-19].

To safeguard the environment, wastewater linked with industrial and textile colors must be cleaned before release by successfully eliminating dye [20-22]. As a result, numerous studies have been conducted to treat dye-contaminated industrial wastewaters using chemical oxidation methods, coagulation and electrocoagulation, Fenton and electro-Fenton oxidation techniques, flocculation, membrane filtration, adsorption, and biological, electrochemical, and photocatalytic treatment methods [23-25]. Among all the ways of decolorization of dyes, the photocatalytic treatment technique is the best choice for dye degradation, with the greatest outcomes for all types of dissolved organic and inorganic material degradation [26, 27]. The photocatalytic technique is a low-cost method that employs semiconductors like TiO2, ZnO, WO3, and CdS, as well as a light source, to form photo-excited carriers, resulting in the generation of hydroxyl radicals, superoxide radical anions, and hydroperoxyl radicals as the main reactive species in photocatalytic oxidation reactions [28, 29]. However, the practical use of photocatalysts is very limited due to the fast recombination rate of photo-generated carriers, and, thereby, many studies have been conducted on the synthesis of nanostructured photocatalysts to decrease the recombination rate of photogenerated charge carriers and promote the practical use of photocatalytic systems for the treatment of wastewater [30, 31].

Direct Red 23 (DR23**;** disodium; 7-[[6-[(4-acetamidophenyl)diazenyl]-5-hydroxy-7-sulfonatonaphthalen-2-yl]carbamoylamino]-4-hydroxy-3-phenyldiazenylnaphthalene-2-sulfonate) is an azo naphtalene dye that is the most frequently used anionic dye in the textile industry. It has been used for cellulose fiber dyeing, also used for silk, wool, paper and pulp dyeing. DR23 has been utilized to the manufacture colors that have pigment [32]. Several studies have been performed to investigate the photocatalytic degradation of DR23 using TiO_2 and ZnO based nanocomposites [33-44]. Some of these dye-photodegradations are based on DR23 oxidation in the presence of hydrogen peroxide [40-44]. This research concentrated on the simple synthesis of low-cost photocatalysts for the degradation of DR23 in the absence of hydrogen peroxide. Therefore, the present work has been focused on the synthesis of GO/Pd/ZnO nanocomposite based on hydrothermal process and its application to the photocatalytic degradation of DR23 from textile wastewater under UV light irradiation.

2. EXPERIMENTAL

2.1. Synthesis of GO/Pd/ZnO nanorods

GO/Pd/ZnO nanorods were synthesized using the hydrothermal method as follows [45]: for synthesis of ZnO nanorods, 50 ml of 30g/l zinc nitrate (98.0%, Shandong Energy Chemical Co., Ltd., China) aqueous solution was added to 10 ml of n-butanol (99.0%, Sigma-Aldrich), and the mixture was magnetically stirred for 120 minutes to obtain a homogenous solution. Next, 20 ml of 1mM sodium citrate (99.0%, Sigma-Aldrich) solution was added to the homogenous solution, and magnetically stirred for 60 minutes. The solution was then stirred for 60 minutes after 2 ml of 0.5 NaOH (99.0%, Shandong Energy Chemical Co., Ltd., China) solution was added. The solution was then transferred to a 100 ml Teflon-lined stainless steel autoclave and heated to 130 °C for 10 hours. After cooling, the resultant precipitates were collected and washed with deionized water and ethanol three times, and dried at 70 °C for 12 hours.

To make Pd/ZnO nanorods, 50 ml of acetone (99.0%, Shandong Baovi Energy Technology Co., Ltd., China) solution was mixed with 1g of prepared ZnO nanorods powder and 1g of palladium nitrate dehydrate (40%, Sigma-Aldrich), which was then calcined at 450 °C for 120 minutes in an argon environment. The GO/Pd/ZnO nanorods were made by ultrasonically mixing 300 mg of Pd/ZnO powder with 20 ml of 5 g/l GO solution (99%, Luoyang Tongrun Info Technology Co., Ltd., China). The suspension was then placed in a 100 mL Teflon-lined stainless steel autoclave and heated to 200°C for 10 hours. The resulting precipitates were washed several times with deionized water and ethanol after hydrothermal reactions, and the GO/Pd/ZnO nanorods were dried in an oven at 85 °C for 8 hours.

2.2. Characterization

The crystal structures of the produced nanorods were studied using an X-ray diffractometer (XRD, Thermo X'TRA X-ray diffractometer employing CuK radiation). Scanning electron microscopy was used to examine the morphology of nanostructures (SEM; JSM-6490LV, Japan). A spectrophotometer was used to measure the UV-visible absorption spectra of the samples (Spectra Max Plus 384, Molecular Devices Co., Sunnyvale, CA). Experiments in electrochemical impedance spectroscopy (EIS) were performed on a potentiostat/galvanostat (Autolab® model PGSTAT 10N, Eco Chemie, Netherlands) with an electrochemical cell containing a ZnO, Pd/ZnO, and GO/Pd/ZnO nanostructures modified glassy carbon electrode (GCE) as the working electrode, a platinum plate as the counter electrode, and an Ag/AgCl electrode as a reference electrode. EIS experiments were carried out in a 0.25 M Na_2SO_4 (≥99%, Sigma-Aldrich) solution by applying an AC voltage of 5 mV in the frequency range from 10^5 Hz to 10^{-2} Hz. The fitting of the result data in EIS experiments and the equivalent circuit were performed using the ZView2 software. For modification of the GCE surface with synthesized nanostructures, 30 g/l of synthesized nanostructure suspension was dropped on the GCE surface and dried at room temperature.

2.3. Study the photocatalytic Activity

The degradation of DR23 under UV irradiation at room temperature using a UV lamp was used to study the photocatalytic performance of photocatalysts (ZnO nanorods, Pd/ZnO nanorods, and GO/Pd/ZnO nanocomposite) (1000W, 365 nm, Hebei Flash Cure Optoelectronic Technology Co., Ltd., China). In a typical procedure, 100 ml of 80 mg/l DR23 (content 30%, Sigma-Aldrich) solution was mixed with 0.5 g/1 photocatalyst. After that, the photocatalyst and DR23 solution were maintained in the dark for one hour to ensure that the DR23 on the photocatalyst surface was in adsorption–desorption equilibrium before irradiation. The combination was then subjected to UV radiation in order to breakdown the DR23 solution. The distance between the surface of the UV lamp and the surface of the DR23 solution was 8 cm. During all photocatalytic measurements, the mixture of photocatalyst and DR23 solution was continuously stirred. After irradiation with UV light at a given time interval, the irradiated samples were filtered through a filter paper (50 μm, Whatman) and centrifuged at 1500 rpm for 10 minutes to remove photocatalyst particles from the dye solution, and the concentration of DR23 in irradiated DR23 solutions was determined using UV-vis absorbance at λ_{max} = 512 nm [33, 46]. The degradation efficiency of the dye can be determined as follows [47, 48]:

$$\text{Degradation efficiency (\%)} = \frac{I_0 - I_t}{I_0} \times 100 = \frac{C_0 - C_t}{C_0} \times 100$$

Where I_o and I_t are the absorbance intensity of the DR23 at initial and after irradiation UV light at time t, and C_o and C_t are the corresponded concentration of the DR23 solution at initial and after irradiation UV light at time t, respectively.

3. RESULTS AND DISCUSSION

3.1. Study of morphology and structure of synthesized nanostructures

The XRD patterns of ZnO nanorods, Pd/ZnO nanorods and GO/Pd/ZnO nanocomposite are exhibited in Figures 1a, 1b, and 1c, respectively. As shown from Figure 1a, the XRD pattern of ZnO nanorods reveals the diffraction peaks at 31.66°, 34.56°, 36.05°, 47.51°, 56.43°, 62.67°, 67.76°, 68.95° and 76.59° which are attributed to (100), (002), (101), (102), (110), (103), (112), (201) and (202) planes of the hexagonal wurtzite structure of ZnO (JCPDS card no. 36–1451) [49, 50]. XRD pattern of Pd/ZnO nanorods in Figure 1b depicts two additional peaks at 40.02° and 46.56° which correspond to (111) and (200) reflections of face centered cubic (fcc) structure of Pd (JCPDS card no. 05-0681) [51], implying the introduction of Pd nanoparticles into the ZnO wurtzite structure. The XRD pattern of the GO/Pd/ZnO nanocomposite in Figure 1c shows one additional peak at 23.35° which is indexed to (002) planes of GO [52, 53].

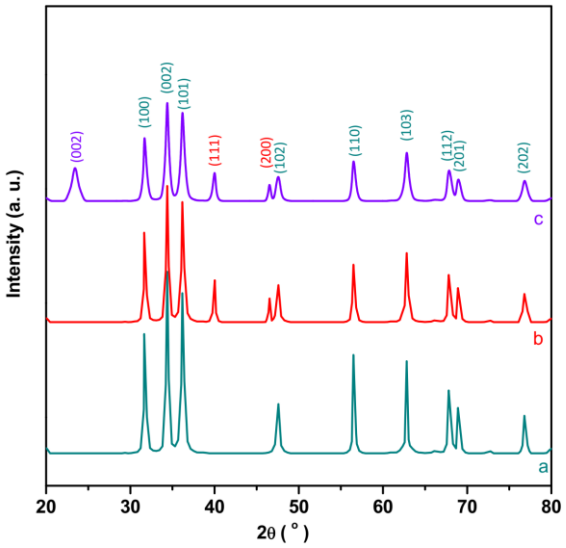

Figure 1. The XRD patterns of (a) ZnO nanorods, (b) Pd/ZnO nanorods and (c) GO/Pd/ZnO nanocomposite.

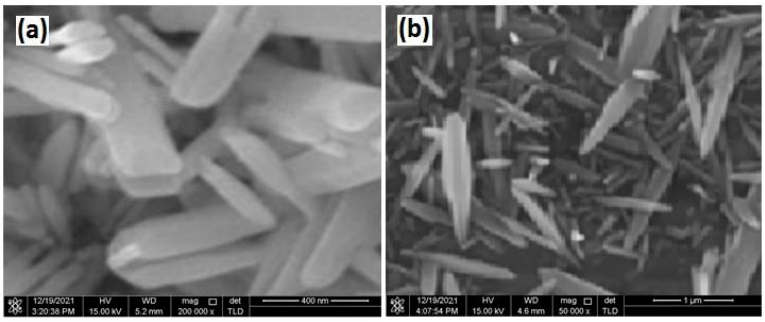

Figure 2. The SEM images of (a) ZnO nanorods, (b) GO/Pd/ZnO nanocomposite.

Figure 2 shows SEM images of ZnO nanorods and GO/Pd/ZnO nanocomposite, respectively. Figure 2a shows a SEM image of ZnO nanorods manufactured in a flawless hexagonal shape with an average diameter of 70 nm. The strong physical bonding between the Pd/ZnO nanorods and GO nanosheets is visible in the SEM images of the GO/Pd/ZnO nanocomposite in Figure 2c. As can be shown, anchoring Pd/ZnO nanorods to GO nanosheets increases porosity and creates more active sites on the nanocomposite's surface, increasing the effective surface area. Furthermore, XRD and SEM studies show that the GO/Pd/ZnO nanocomposite was successfully synthesized.

3.2. Study of optical properties

Figure 3a shows the UV-visible absorption spectra of ZnO nanorods, Pd/ZnO nanorods and GO/Pd/ZnO nanocomposite. As observed, the absorption edges of Pd/ZnO nanorods and GO/Pd/ZnO nanocomposite are slightly red-shifted toward the pure ZnO nanorods which is associated with two integrative factors [54, 55]: (i) the formation of impurity levels near the valence band and the formation of defect states such as oxygen vacancies, zinc vacancies, zinc interstitials, and oxygen

interstitials as trapped states that act as electron sinks, lowering the recombination rate of photo-excited holes in the valance band and electrons in the conduction band and extending the lifetime of photo-excited charge carriers, thereby improving photocatalytic performance [56, 57]. Moreover, oxygen vacancy defects are useful for improving light absorption of the ZnO matrix due to the presence of the d–d transition of free Zn [58]. (ii) The intimate interfacial interaction between Pd, GO and ZnO. Studies have indicated that the interaction between the surface defects of ZnO and the π-electron of GO, and π–π* transition of aromatic C–C bonds and n→π* transitions of C=O bonds of GO in the nanocomposite structure can lead to a red-shift of the absorption band-edge [59, 60]. Certainly, the red-shift of the light absorption edge to the visible light region reveals that the GO/Pd/ZnO nanocomposite could present the photocatalytic activity under visible light irradiation [54, 61]. On the other hand, reports have indicated that the conduction band and valence band of ZnO are -4.05 eV and -7.25 eV, respectively, and the work functions of GO is −4.42 eV. Thus, on the basis of the relevant band positions of ZnO and GO, photo-excited electrons easily transfer from the ZnO conduction band to GO, implying the efficient separation of the photo-excited electron and holes and hindering the charge recombination in electron-transfer processes [53, 62]. Figure 3b shows the Tauc plot of ZnO nanorods, Pd/ZnO nanorods and GO/Pd/ZnO nanocomposite which is used for the determination of band gap value of samples through the following formula [63-65]:

$$(\alpha h\nu)^2 = B(h\nu - E) \qquad (2)$$

Where hν and α and hν are absorbance and photon energy, respectively. B is the proportionality constant and E refers to the optical band gap. The optical band gap is obtained by extrapolating the linear part of curve $(\alpha h\nu)^2$ as a function of the intercept energy X axis (hν). As found, the optical band gap values are obtained at 3.10, 3.01 and 2.95 eV for ZnO nanorods, Pd/ZnO nanorods and GO/Pd/ZnO nanocomposite, respectively, indicating the GO/Pd/ZnO nanocomposite exhibits a narrower band gap when compared to pure ZnO and Pd/ZnO nanorods. This phenomenon can be explained by the formation of Zn–O–C chemical bonds in the GO/Pd/ZnO nanocomposite [60, 66]. Incorporation of Pd metal and GO as conductive nanomaterials narrows the band gap of nanocomposite and extends light absorption to longer wavelengths [53, 58]. High conductivity also inhibits recombination and the longer wavelength light absorption can lead to a larger number of photo-generated electrons from valence to conduction band.

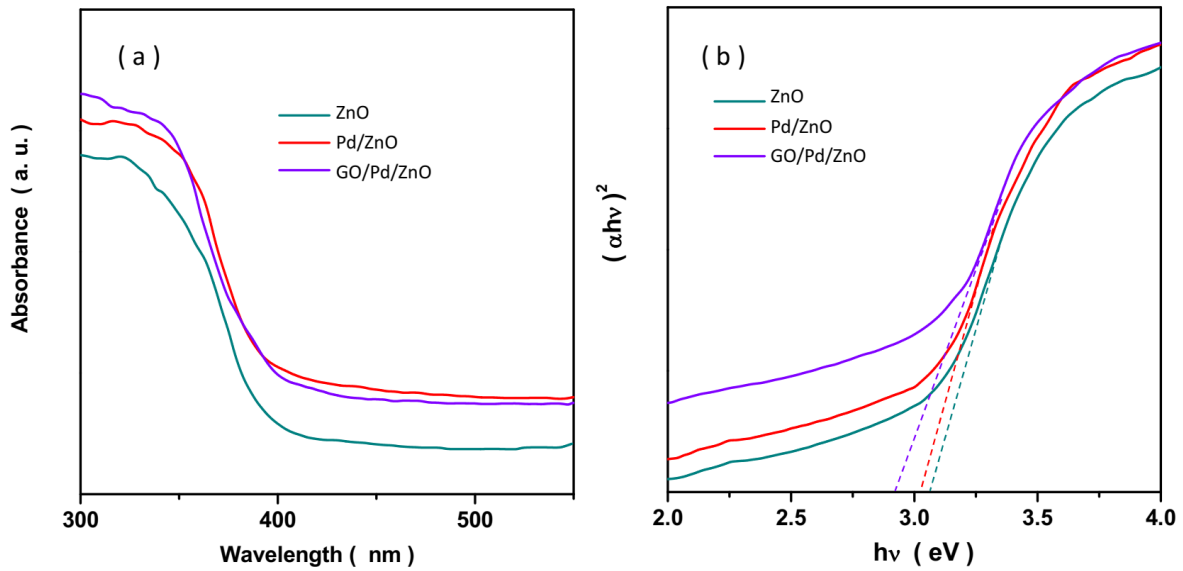

Figure 3. (a) UV-visible absorption spectra and (b) Tauc plot of ZnO nanorods, Pd/ZnO nanorods and GO/Pd/ZnO nanocomposite.

3.3. Electrochemical study

By applying an AC voltage of 5 mV in the frequency range of 10^5 Hz to 10^{-2} Hz, EIS studies were conducted to study the impedance properties and charge transfer across the synthesized photocatalysts in a 0.25 M Na2SO4 solution. The Nyquist plots are shown in Figure 4a, with semicircle curves for all samples in the high frequency range, followed by an inclined line in the low frequency region. The resistance to electron passage at the interface is proportional to the diameter of the semicircle. As can be seen, the semicircle radius of ZnO nanorods is the biggest, signifying the strongest charge transfer resistance. A significant decrease in the semicircle radius is observed for Pd/ZnO nanorods and especially for GO/Pd/ZnO nanocomposite. The equivalent circuit and the results of fitting parameters for Nyquist plots are presented in the inset of Figure 4a and Table 2 which contains Rt as charge transfer resistance, R_S as electrolyte resistance, Cdl as double layer capacitor, Zw as Warburg impedance referred to an inclined straight line at the low frequency range that is characteristic of the diffusion-limiting step of the electrochemical process [67-69]. Due to the use of the same electrolyte in all samples, the Rs value was found to be nearly constant. Furthermore, studies show that adding Pd and GO nanosheets to the ZnO structure increases capacitance and decreases R_t, implying that the charge carrier transfer rate is improved and charge recombination is reduced.

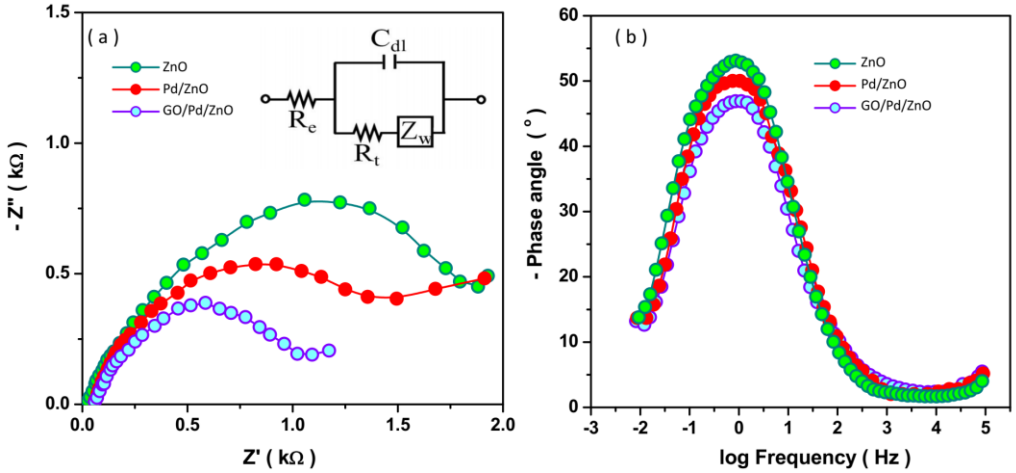

Figure 4. (a) Nyquist plots (inset: used equivalent circuit) and (b) bode plots.

Table 1. The obtained values for fitting data of the circuit elements.

Sample	Rs(Ω)	C_{dl} (nF)	R_t (kΩ)
ZnO	32.02	1.29	1.982
Pd/ZnO	32.63	1.49	1.701
GO/Pd/ZnO	31.61	1.50	1.198

On the other hand, it could be related to the GO/Pd/ZnO nanocomposite's outstanding separation and transfer of photo-excited charge carriers [70, 71]. Figure 4b shows the obtained Bode plots of ZnO nanorods, Pd/ZnO nanorods and GO/Pd/ZnO nanocomposite which contain one phase angle peak corresponding to one constant time at the frequency range from 1 to 10^2 Hz, and indicating that the electron transfer processes occurred at the electrode/electrolyte interface [72, 73].

3.4. Study the photocatalytic performance

Figure 5 depicts the findings of the research on the photocatalytic activity of ZnO nanorods, Pd/ZnO nanorods, and GO/Pd/ZnO nanocomposite for the degradation of 100 ml of 80 mg/l DR23 solution in darkness and UV light. Figures 5a and 5b, respectively, indicate the deterioration efficiency in terms of time under UV light irradiation. To investigate the effect of light and photocatalyst on DR23 degradation, the degradation efficiency in terms of time under dark for all samples (in the first 60 minutes) is less than 0.85%, while the degradation efficiency in the absence of photocatalyst (blank sample) is 1.95% after 170 minutes in the dark. However, the remarkable degradation is observed after irradiation with UV light in the first minutes, as observed from Figure 5a, the degradation efficiency is obtained 10.2%, 15.3% and 26.7% using ZnO nanorods, Pd/ZnO nanorods and GO/Pd/ZnO nanocomposite after 10 minutes of irradiation with UV light, respectively. These observations reveal the great roles of UV light and photocatalysts in the degradation of DR23 solution.

Furthermore, Figure 5a shows that after 60 minutes of UV light irradiation, ZnO nanorods, Pd/ZnO nanorods, and GO/Pd/ZnO nanocomposite have 63.0%, 75.9%, and 84.7% DR23 degradation efficiency, respectively, and complete treatment is achieved after 145, 125, and 120 minutes of UV light irradiation on ZnO nanorods, Pd/ZnO nanorods, As can be seen from the photocatalytic activity of the samples, the GO/Pd/ZnO nanocomposite has a higher rate of dye degradation, which can be attributed to its improved surface roughness and porosity, which increases the overall surface area and thus the exposed surface area towards the light source, and thus increases the overall active site surface area available for photocatalytic degradation [74-76]. The photocatalytic degradation of DR23 may occur according to the following mechanism: First, when a photon irradiates a photocatalytic system, the photon energy (hν) is equal to or higher than the band gap of the semiconductor, an electron in the valence band can be excited to the conduction band with the simultaneous generation of a hole in the valence band. The photo-excited electron and hole pair result in the generation of hydroxyl radicals, superoxide radical anions and hydroperoxyl radicals, which are the main reactive species in photocatalytic oxidation reactions [77, 78]. The incorporation of GO nanosheets and Pd particles into the ZnO structure narrows the band gap of the nanocomposite, resulting in the formation of defects states and impurity levels in the conduction band and near the valence band that act as trapping centers for photo-generated electrons, effectively separating the photo-generated electron–hole pairs and resulting in high photocatalytic activity [79]. The presence of GO nanosheets and Pd particles in nanocomposite, results in higher hydroxide and superoxide radical concentrations and enhances the photocatalytic activity [56]. It is found that the photocatalytic studies results are in good accordance with SEM, EIS and optical studies.

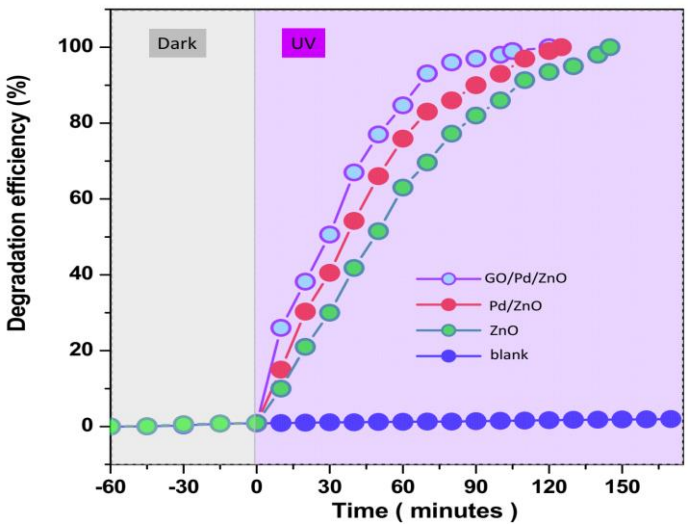

Figure 5. The photocatalytic activity of ZnO nanorods, Pd/ZnO nanorods and GO/Pd/ZnO nanocomposite for degradation of 100 ml of 80 mg/l DR23 solution under darkness and UV light irradiation

Table 2 compares the performance of various photocatalysts reported in the literature with that of this study for the degradation of DR23, indicating that the GO/Pd/ZnO nanocomposite has a high photocatalytic efficiency due to the synergetic action of GO, Pd, and ZnO, as well as efficient

separation of electron–hole pairs due to the formation of an intermediate band in the nanocomposite's energy band-gap.

Table 2. Comparison between performance of reported different photocatalysts in the literatures and this study for degradation of DR23.

Photocatalyst	DR23 **content (mg/l)**	**Light source**	**Degradation time (minute)**	**Removal efficiency (%)**	**Ref.**
GO/Pd/ZnO	80	UV	120	100	This work
Pd/ZnO			125	100	
ZnO			145	100	
Ag-doped TiO_2	162	UV	20	54	[34]
TiO_2	122	UV	360	97.9	[39]
Ce-doped ZnO	40	UV	70	99.5	[33]
ZnO	40	UV	110	100	[36]
$InVO_4$–TiO_2	20	visible	60	94	[35]
TiO_2	20	UV	180	54.2	[37]
$TiO_2/S_2O_8^{2-}$	20	UV	35	89.9	[38]

In a prepared genuine sample of textile wastewater, the usefulness of the produced photocatalysts for the degradation of DR23 was studied. Figure 6 shows the photocatalytic activity of ZnO nanorods, Pd/ZnO nanorods, and GO/Pd/ZnO nanocomposite for the degradation of a 100 ml of 80 mg/l DR23 solution prepared from a real sample of textile wastewater under UV light irradiation, with complete treatment after 155, 135, and 125 minutes, respectively. As seen, the degradation rate of a prepared real is different on three photocatalysts, and the fastest complete degradation of prepared real sample occurred on GO/Pd/ZnO nanocomposite (125 minutes), and the slowest degradation is obtained using ZnO nanorods (155 minutes). Figure 5 (dye solution prepared with deionized water) and Figure 6 (total treatment of dye solution prepared real sample of textile wastewater) show that total treatment of dye solution prepared with a real sample of textile wastewater requires more time on all photocatalyst, which can be attributed to the presence of organic and inorganic pollutants in wastewater. According to the findings, the photocatalyst produced in this work can be used to remediate the DR23 pollutant in textile wastewater.

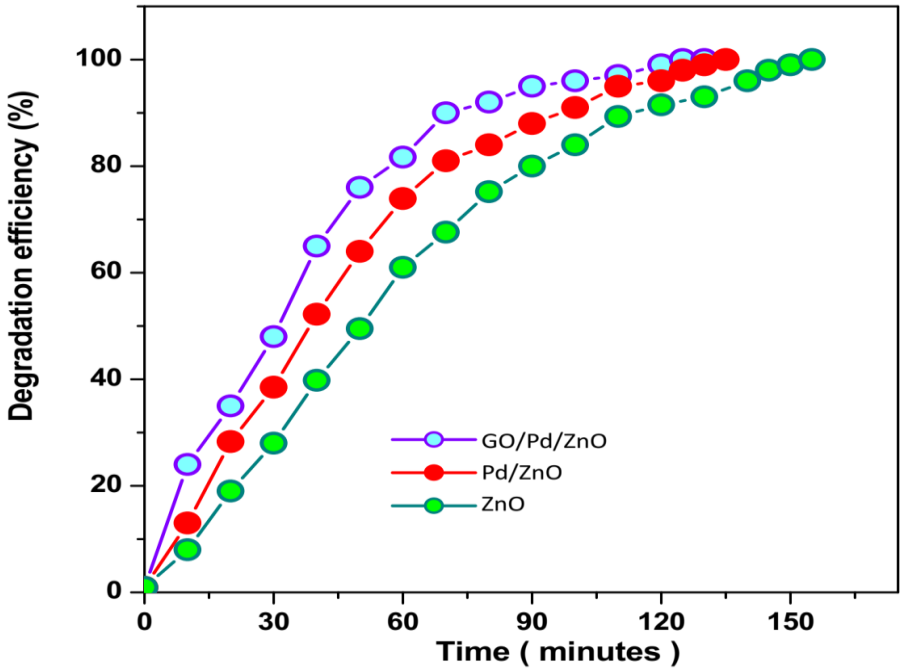

Figure 6. The photocatalytic performance of ZnO nanorods, Pd/ZnO nanorods and GO/Pd/ZnO nanocomposite for degradation of 100 ml of 80 mg/l DR23 solution prepared real sample of textile wastewater under UV light irradiation.

4. CONCLUSION

In this study, the hydrothermal production of GO/Pd/ZnO nanocomposite and its application to the photocatalytic degradation of DR23 from textile wastewater under UV light irradiation were presented. The Pd/ZnO nanorods anchored onto the crumpled-like characteristics of the GO nanosheets, revealing the strong physical connection between the Pd/ZnO nanorods and GO nanosheets, according to the results of structural investigations. The absorption edges of Pd/ZnO nanorods and GO/Pd/ZnO nanocomposite were slightly red-shifted toward pure ZnO nanorods, and the optical band gap values for ZnO nanorods, Pd/ZnO nanorods, and GO/Pd/ZnO nanocomposite were 3.10, 3.01, and 2.95 eV, respectively, indicating that the GO/Pd/ZnO nanocomposite exhibits a narrower band gap when compared to pure ZnO and Pd/ZnO nanorods. With the addition of Pd and GO nanosheets to the ZnO structure, EIS measurements revealed a reduction in charge transfer resistance, indicating that the charge carrier transfer rate and charge recombination in the GO/Pd/ZnO nanocomposite are improved. Study the photocatalytic performance of photocatalysts for degradation of 100 ml of 80 mg/l DR23 solution under UV light irradiation showed that 63.0%, 75.9% and 84.7% degradation efficiency of DR23 is obtained for ZnO nanorods, Pd/ZnO nanorods and GO/Pd/ZnO nanocomposite after 60 minutes of UV light irradiation, respectively, and complete treatment is attained after 145, 125 and 120 minutes UV light irradiation on ZnO nanorods, Pd/ZnO nanorods and GO/Pd/ZnO nanocomposite, respectively, indicated to great photocatalytic efficiency of GO/Pd/ZnO nanocomposite compared to reported different photocatalysts in the literature because of the synergetic action between GO, Pd and ZnO, and efficient separation of the electron–hole pairs due to formation

of intermediate band in energy band-gap of nanocomposite. Results showed that the developed photocatalysts in this study can be used for the treatment of the DR23 pollutant in textile wastewater.

ACKNOWLEDGMENTS
The authors are grateful for the financial support provided by the Chemical and environmental science and technology innovation team (No. ybzy20cxtd03), and the scientific research project of Yibin Vocational Technical College (Grant No. ybzysc20-07).

References

1. S. Benkhaya, S. M'rabet and A. El Harfi, *Inorganic Chemistry Communications*, 115 (2020) 107891.
2. T. Zhang, X. Wu, S.M. Shaheen, H. Abdelrahman, E.F. Ali, N.S. Bolan, Y.S. Ok, G. Li, D.C. Tsang and J. Rinklebe, *Journal of hazardous materials*, 425 (2022) 127906.
3. H. Karimi-Maleh, H. Beitollahi, P.S. Kumar, S. Tajik, P.M. Jahani, F. Karimi, C. Karaman, Y. Vasseghian, M. Baghayeri and J. Rouhi, *Food and Chemical Toxicology*, (2022) 112961.
4. C. Pan, Z. Mao, X. Yuan, H. Zhang, L. Mei and X. Ji, *Advanced Science*, 25 (2022) 2105747.
5. Y. Liu, Q. Zhang, H. Yuan, K. Luo, J. Li, W. Hu, Z. Pan, M. Xu, S. Xu and I. Levchenko, *Journal of Alloys and Compounds*, 868 (2021)
6. S.M. Burkinshaw and G. Salihu, *Dyes and Pigments*, 161 (2019) 531.
7. M. Cao, Z. Chang, J. Tan, X. Wang, P. Zhang, S. Lin, J. Liu and A. Li, *ACS Applied Materials & Interfaces*, 14 (2022) 13025.
8. L. He, M.-X. Li, F. Chen, S.-S. Yang, J. Ding, L. Ding and N.-Q. Ren, *Journal of hazardous materials*, 417 (2021) 126113.
9. S. Guo, C. Li, Y. Zhang, Y. Wang, B. Li, M. Yang, X. Zhang and G. Liu, *Journal of Cleaner Production*, 140 (2017) 1060.
10. K.A. Zahidah, S. Kakooei, M. Kermanioryani, H. Mohebbi, M.C. Ismail and P.B. Raja, *International Journal of Engineering and Technology Innovation*, 7 (2017) 243.
11. S. Velusamy, A. Roy, S. Sundaram and T. Kumar Mallick, *The Chemical Record*, 21 (2021) 1570.
12. C.-X. Chen, S.-S. Yang, J. Ding, G.-Y. Wang, L. Zhong, S.-Y. Zhao, Y.-N. Zang, J.-Q. Jiang, L. Ding and Y. Zhao, *Applied Catalysis B: Environmental*, 298 (2021) 120495.
13. J. Rouhi, C.R. Ooi, S. Mahmud and M.R. Mahmood, *Materials Letters*, 147 (2015) 34.
14. L. Feng, J.J. Liu, Z.C. Guo, T.Y. Pan, J.H. Wu, X.H. Li, B.Z. Liu and H.L. Zheng, *Separation and Purification Technology*, 285 (2021)120314.
15. C. Shi, Z. Wu, F. Yang and Y. Tang, *Solid State Sciences*, 119 (2021) 106702.
16. M. Yang, C. Li, Y. Zhang, D. Jia, R. Li, Y. Hou and H. Cao, *The International Journal of Advanced Manufacturing Technology*, 102 (2019) 2617.
17. R. Kishor, D. Purchase, G.D. Saratale, R.G. Saratale, L.F.R. Ferreira, M. Bilal, R. Chandra and R.N. Bharagava, *Journal of Environmental Chemical Engineering*, 9 (2021) 105012.
18. W. Liu, F. Huang, Y. Liao, J. Zhang, G. Ren, Z. Zhuang, J. Zhen, Z. Lin and C. Wang, *Angewandte Chemie*, 120 (2008) 5701.
19. M. Yang, C. Li, Y. Zhang, D. Jia, R. Li, Y. Hou, H. Cao and J. Wang, *Ceramics International*, 45 (2019) 14908.
20. E. Islam, D. Liu, T. Li, X. Yang, X. Jin, Q. Mahmood, S. Tian and J. Li, *Journal of hazardous materials*, 154 (2008) 914.

21. J. Liu, Q. Zhang, X. Tian, Y. Hong, Y. Nie, N. Su, G. Jin, Z. Zhai and C. Fu, *Chemical Engineering Journal*, 404 (2021) 127146.
22. H. Karimi-Maleh, C. Karaman, O. Karaman, F. Karimi, Y. Vasseghian, L. Fu, M. Baghayeri, J. Rouhi, P. Senthil Kumar and P.-L. Show, *Journal of Nanostructure in Chemistry*, (2022) 1.
23. A. Ahmad, S.H. Mohd-Setapar, C.S. Chuong, A. Khatoon, W.A. Wani, R. Kumar and M. Rafatullah, *RSC advances*, 5 (2015) 30801.
24. L. Feng, X.H. Li, W.C. Lu, Z. Liu, C. Xu, Y.N. Chen, H.L. Zheng, *International Journal of Biological Macromolecules*, 150 (2020) 617.
25. M. Nazeer, F. Hussain, M.I. Khan, E.R. El-Zahar, Y.-M. Chu and M. Malik, *Applied Mathematics and Computation*, 420 (2022) 126868.
26. J. Zhang, C. Li, Y. Zhang, M. Yang, D. Jia, G. Liu, Y. Hou, R. Li, N. Zhang and Q. Wu, *Journal of cleaner production*, 193 (2018) 236.
27. H. Karimi-Maleh, R. Darabi, M. Shabani-Nooshabadi, M. Baghayeri, F. Karimi, J. Rouhi, M. Alizadeh, O. Karaman, Y. Vasseghian and C. Karaman, *Food and Chemical Toxicology*, 162 (2022) 112907.
28. B. Li, C. Li, Y. Zhang, Y. Wang, D. Jia and M. Yang, *Chinese Journal of Aeronautics*, 29 (2016) 1084.
29. M. Husairi, J. Rouhi, K. Alvin, Z. Atikah, M. Rusop and S. Abdullah, *Semiconductor Science and Technology*, 29 (2014) 075015.
30. K. Bramhaiah and S. Bhattacharyya, *Materials Advances*, 3 (2022) 142.
31. M. Alimanesh, J. Rouhi and Z. Hassan, *Ceramics International*, 42 (2016) 5136.
32. J. Rouhi, S. Mahmud, S. Hutagalung and S. Kakooei, *Micro & Nano Letters*, 7 (2012) 325.
33. R. Kumar, A. Umar, G. Kumar, M. Akhtar, Y. Wang and S. Kim, *Ceramics International*, 41 (2015) 7773.
34. N. Sobana, K. Selvam and M. Swaminathan, *Separation and Purification Technology*, 62 (2008) 648.
35. S. Dianat, *Iranian Journal of Catalysis*, 8 (2018) 121.
36. G. Kumar, R. Kumar, S.W. Hwang and A. Umar, *Journal of nanoscience and nanotechnology*, 14 (2014) 7161.
37. N. Daneshvar, D. Salari, A. Niaei, M. Rasoulifard and A. Khataee, *Journal of Environmental Science and Health, Part A*, 40 (2005) 1605.
38. M. Rasoulifard, M. Fazli and M. Eskandarian, *Journal of Industrial and Engineering Chemistry*, 20 (2014) 3695.
39. D.N. Clausen, I.S. Scarminio and K. Takashima, *Journal of the Chilean Chemical Society*, 54 (2009) 289.
40. N. Danyliuk, T. Tatarchuk, K. Kannan and A. Shyichuk, *Water Science and Technology*, 84 (2021) 469.
41. N.M. Mahmoodi, *Water, Air, & Soil Pollution*, 224 (2013) 1.
42. M. Torkaman, R. Moradi and B. Keyvani, *Rev Roum Chim*, 61 (2016) 763.
43. N.M. Mahmoodi, M. Arami, N.Y. Limaee and N.S. Tabrizi, *Chemical Engineering Journal*, 112 (2005) 191.
44. J. Cheng, G. Gu, W. Ni, Q. Guan, Y. Li and B. Wang, *Nanotechnology*, 28 (2017)
45. Y.-H. Zhang, Y.-L. Li, X.-R. Shen, K.-F. Xie, T.-Y. Li, J.-N. Zhao, Q.-J. Jia, F.-L. Gong and S.-M. Fang, *Journal of Physics and Chemistry of Solids*, 136 (2020) 109144.
46. H. Yan, M. Zhao, X. Feng, S. Zhao, X. Zhou, S. Li, M. Zha, F. Meng, X. Chen and Y. Liu, *Angewandte Chemie*, (2022) 1.
47. X. Chen, Z. Wu, D. Liu and Z. Gao, *Nanoscale Research Letters*, 12 (2017) 143.
48. Y.-M. Chu, B. Shankaralingappa, B. Gireesha, F. Alzahrani, M.I. Khan and S.U. Khan, *Applied Mathematics and Computation*, 419 (2022) 126883.

49. E. de Lucas-Gil, J. Menendez, L. Pascual, J.F. Fernandez and F. Rubio-Marcos, *Applied Sciences*, 10 (2020) 1322.
50. H. Savaloni and R. Savari, *Materials Chemistry and Physics*, 214 (2018) 402.
51. P. Eghbali, B. Nişancı and Ö. Metin, *Pure and Applied Chemistry*, 90 (2018) 327.
52. C. Ma, K. Yang, L. Wang and X. Wang, *Journal of Applied Biomaterials & Functional Materials*, 15 (2017) 1.
53. R. Savari, J. Rouhi, O. Fakhar, S. Kakooei, D. Pourzadeh, O. Jahanbakhsh and S. Shojaei, *Ceramics International*, 47 (2021) 31927.
54. X. Pan, M.-Q. Yang and Y.-J. Xu, *Physical Chemistry Chemical Physics*, 16 (2014) 5589.
55. R. Hassanzadeh, A. Siabi-Garjan, H. Savaloni and R. Savari, *Materials Research Express*, 6 (2019) 106429.
56. N. Güy, S. Çakar and M. Özacar, *Journal of Colloid and Interface Science*, 466 (2016) 128.
57. R. Mohamed, J. Rouhi, M.F. Malek and A.S. Ismail, *International Journal of Electrochemical Science*, 11 (2016) 2197.
58. M.M. Hossain, B.-C. Ku and J.R. Hahn, *Applied Surface Science*, 354 (2015) 55.
59. I. Boukhoubza, M. Khenfouch, M. Achehboune, L. Leontie, A.C. Galca, M. Enculescu, A. Carlescu, M. Guerboub, B.M. Mothudi and A. Jorio, *Nanomaterials*, 10 (2020) 1532.
60. H.N. Tien, N.T. Khoa, S.H. Hahn, J.S. Chung, E.W. Shin and S.H. Hur, *Chemical engineering journal*, 229 (2013) 126.
61. L. He, C. Yang, J. Ding, M.-Y. Lu, C.-X. Chen, G.-Y. Wang, J.-Q. Jiang, L. Ding, G.-S. Liu and N.-Q. Ren, *Applied Catalysis B: Environmental*, 303 (2022) 120880.
62. T. Lv, L. Pan, X. Liu and Z. Sun, *Catalysis Science & Technology*, 2 (2012) 2297.
63. M. Wang, S. Yuan, B. Lv and H. Yang, *International Journal of Electrochemical Science*, 16 (2021) 210248.
64. T. Murakami and T. Abe, *International Journal of Electrochemical Science*, 15 (2020) 7381.
65. T.H. Zhao, M.I. Khan and Y.M. Chu, *Mathematical Methods in the Applied Sciences*, (2021) 1.
66. J. Rouhi, S. Kakooei, S.M. Sadeghzadeh, O. Rouhi and R. Karimzadeh, *Journal of Solid State Electrochemistry*, 24 (2020) 1599.
67. E. Hür, G.A. Varol and A. Arslan, *Synthetic Metals*, 184 (2013) 16.
68. D. Zhang, C. Li, Y. Zhang, D. Jia and X. Zhang, *The International Journal of Advanced Manufacturing Technology*, 78 (2015) 1275.
69. N. Naderi, M. Hashim, J. Rouhi and H. Mahmodi, *Materials science in semiconductor processing*, 16 (2013) 542.
70. C. Chen, X. Liu, Q. Fang, X. Chen, T. Liu and M. Zhang, *Vacuum*, 174 (2020) 109198.
71. H. Maleh, M. Alizadeh, F. Karimi, M. Baghayeri, L. Fu, J. Rouhi, C. Karaman, O. Karaman and R. Boukherroub, *Chemosphere*, (2021) 132928.
72. T. Lopes, L. Andrade, H.A. Ribeiro and A. Mendes, *international journal of hydrogen energy*, 35 (2010) 11601.
73. Y. Hu, G. Yang, J. Zhou, H. Li, L. Shi, X. Xu, B. Cheng and X. Zhuang, *ACS nano*, (2022) 1.
74. S.H. Mohamed Noor, M.H.D. Othman, W. Khongnakorn, O. Sinsamphanh, H. Abdullah, M.H. Puteh, T.A. Kurniawan, H.S. Zakria, T. El-badawy and A.F. Ismail, *Membranes*, 12 (2022) 208.
75. Z. Savari, S. Soltanian, A. Noorbakhsh, A. Salimi, M. Najafi and P. Servati, *Sensors and Actuators B: Chemical*, 176 (2013) 335.
76. H. Savaloni, E. Khani, R. Savari, F. Chahshouri and F. Placido, *Applied Physics A*, 127 (2021) 1.
77. M.O. Pacheco-Álvarez, O.M. Rodríguez-Narváez, K. Wrobel, R. Navarro-Mendoza, J.N.-M. de Oca and J.M. Peralta-Hernández, *International Journal of Electrochemical Science*, 13 (2018) 11549.

78. Y.-M. Chu, U. Nazir, M. Sohail, M.M. Selim and J.-R. Lee, *Fractal and Fractional*, 5 (2021) 119.
79. J. Chen, D. Yang, D. Song, J. Jiang, A. Ma, M.Z. Hu and C. Ni, *Journal of Power Sources*, 280 (2015) 649.